applied sciences

MDPI

Article

Modified Solution–Diffusion Model Incorporating Rotational Kinetic Energy in Pressure Retarded Osmosis

Daniel Ruiz-Navas [1,2], Edgar Quiñones-Bolaños [2] and Mostafa H. Sharqawy [1,*]

[1] School of Engineering, University of Guelph, Guelph, ON N1G 2W1, Canada; druizn@unicartagena.edu.co
[2] Faculty of Engineering, University of Cartagena, Cartagena 131001, Colombia; equinonesb@unicartagena.edu.co
* Correspondence: melsharq@uoguelph.ca

Abstract: Pressure-retarded osmosis (PRO) is a process that allows the production of mechanical energy from the chemical potential difference between two solutions of different concentrations separated by a semi-permeable membrane. One of the main obstacles for this technology to be commercially competitive is the difference between the theoretical power density and the experimental power density due to negative factors like ICP. Analytical models facilitate the analysis of the relationships between system parameters and thus facilitate the optimization of components. In general, PRO has traditionally been explained through the solution–diffusion model, where the flow of water through the membrane depends on a diffusivity factor, the concentration gradient, and the hydraulic pressure gradient. This paper focuses on developing a modified solution–diffusion model that includes means to control the ICP through rotational kinetic energy. An energy balance method for obtaining a solution diffusion-based model is explained, and an analytical model is obtained. Finally, said model is verified through simulations with parameters reported in the literature to obtain insight on the required dimensions for a prototype. It was found that a turning radius of 0.5 m and an angular speed of less than 3000 rev/min could generate enough kinetic energy to compensate for ICP losses in a PRO scenario. Also, the results suggest that bigger concentration differences could benefit more of this technology, as they require almost the same energy as smaller concentration differences but allow for more energy extraction.

Keywords: pressure-retarded osmosis; solution–diffusion model; rotational kinetic energy

check for updates

Academic Editor: Nikolaos Koukouzas

Received: 8 October 2024
Revised: 18 December 2024
Accepted: 22 December 2024
Published: 27 January 2025

Citation: Ruiz-Navas, D.; Quiñones-Bolaños, E.; Sharqawy, M.H. Modified Solution–Diffusion Model Incorporating Rotational Kinetic Energy in Pressure Retarded Osmosis. *Appl. Sci.* **2025**, *15*, 1312. https://doi.org/10.3390/app15031312

Copyright: © 2025 by the authors. Licensee MDPI, Basel, Switzerland. This article is an open access article distributed under the terms and conditions of the Creative Commons Attribution (CC BY) license (https://creativecommons.org/licenses/by/4.0/).

1. Introduction

Power generation using pressure-retarded osmosis (PRO) has garnered significant due to its potential for sustainable and continuous electricity generation. However, several technical challenges related to its practical implementation remain unresolved [1]. Among these challenges is internal concentration polarization (ICP), which is one of the most critical issues that need to be addressed [2].

ICP is a phenomenon that depends on the feed and draw solution concentrations as well as on the structural parameters of the membrane. Its effects could be minimized from the design of the membrane itself or by maintaining operating conditions that help mitigate its effects [3].

In PRO, as well as in various other membrane processes, a high shear rate induced by turbulence near the membrane surface is desirable. This turbulence enhances water flux flow through the membrane and mitigates the effects of concentration polarization (CP) and reduces membrane fouling [4–8]. The use of high-velocity flow rates generates this

turbulence, but the required working pressures of PRO and the use of high-velocity flow rates requires more energy from the pumps, diminishing the net energy output.

There is some research on other membrane processes that have employed rotational kinetic energy to produce high shear rates in the area near the membrane. The work of Wild et al. in [9] defines the fundamental principles and implements two prototypes of centrifugal reverse osmosis (CRO). Pharoah et al., in [10], studies the favorable effects of centrifugal and Coriolis acceleration for a centrifugal membrane separation (CMS) process are evaluated with a numerical model. Bergen et al., in [11], experiments to evaluate the use of CMS to enhance water flux in rotating reverse osmosis (RO) are presented. Lee and Lueptow, in [12], present a dynamic model for rotating reverse osmosis with the Navier–Stokes equation for cylindrical Taylor–Couette flow. The same authors, in [13], evaluate the control of scale formation in rotating reverse osmosis. More recently, Krantz and Chong, in [14], present a CRO process that can reduce the specific energy consumption relative to a single-stage RO process by progressively adjusting the trans-membrane pressure with a set radius and a variable speed.

Some studies have explored the technical challenges and energy consumption associated with applying rotational kinetic energy to membrane processes. Experimental, mathematical, and numerical evidence suggests that rotational kinetic energy can help mitigate the negative effects of CP and membrane fouling in these processes. Furthermore, these benefits can be achieved with lower energy consumption.

Due to the similarities between membrane-based processes, many of the technologies developed for RO have been adapted for use in PRO. It could be of interest to evaluate the effects of rotational kinetic energy applied to PRO.

A literature review focused on the mathematical models used specifically for PRO revealed that three fundamental theories have been used to develop models: the solution–diffusion model, irreversible thermodynamics, and mass interchange (See Table A1).

Among the three fundamental theories, the solution–diffusion model is the most used for PRO. In broad terms, permeation through a membrane is defined by driving forces like pressure, temperature, and concentration. These forces are interrelated between them, and the resulting driving force is the gradient of the chemical potential μ [15].

Regarding the process for obtaining the solution–diffusion model, it is highlighted that to calculate the chemical potential μ, usually, only the concentration, temperature, and pressure gradients are considered.

Let us consider that other driving forces, like electromagnetic fields, gravity, or inertia, are present and may directly or indirectly influence the distribution of species and thus the chemical potential of solutions. With this, it is possible to develop new expressions to explain osmotic processes.

Suppose, for example, that, instead of a traditional static PRO system, we have a PRO system that can rotate with a defined angular velocity. Depending on the membrane orientation, there will be effects related to centrifugal and Coriolis forces that could enhance mass transfer through the membrane.

In this work, we present a theoretical system that allows a PRO process to include rotational kinetic energy, and we describe the mathematical method used for obtaining a new expression for a solution–diffusion model affected by rotational kinetic energy.

A PRO system that incorporates rotational kinetic energy can induce turbulence through inertial effects on the feed and draw solutions throughout the entire volume of the membrane module. This turbulence could enhance water flow across the membrane, even in flow-dead zones within the module.

In the proposed PRO system, the membrane module will rotate in the air, moving only the mass of the module and the volume of water inside. As a result, the efficiency of the

electric motor may exceed that of the two hydraulic pumps, which must maintain a high flow rate throughout the entire hydraulic system of the feed and draw solutions in a typical PRO system.

The magnitude of the effects will depend on parameters such as the turning radius, angular velocity, direction of rotation, and solution densities. These factors provide numerous options for controlling the performance of the system.

This theoretical work provides a framework for advancing PRO technology by introducing the possibility of actively controlling CP through rotational kinetic energy. The technical challenges related to the rotating mechanism and couplings, large-scale implementation, and detailed energy consumption of the rotational components are beyond the scope of this study and will be addressed in future research.

2. Considering Other Impulse Forces

Generally speaking, in osmotic processes, the most significant impulse forces are the concentration potential and the convective potential as expressed by Equation (A1). Nonetheless, other kinds of forces could affect these processes. For example, the author Nagy, in [16], presents an equation for the chemical potential of solutions with ionic flows where the electric field is considered an important impulse force.

$$\mu_i = \mu_i^0 + R\ T\ln(a_i) + \hat{v}_i(P) + F_z\ E \tag{1}$$

where a is the activity of component i, F_z is the Faraday constant, and E is the electrical potential.

The driving forces in osmotic processes can vary depending on the specific parameters of the process or the physical properties of the system. In certain cases, additional forces can be considered, such as the chemical potential of a solution influenced by a sufficiently strong electromagnetic field, gravitational forces, or kinetic energy. These factors can be mathematically expressed as follows:

$$\mu_i = \left[\mu_i^0 + R\ T\ln\left(\frac{\gamma_i\ C_i}{\rho_i\ m_i}\right)\right]_{Ec} + [\hat{v}_i.(P_i - P_{sati})]_{Ef} + [F_z\ E_i]_{Ee} + [m_i g\ h]_{Ep} + \left[\frac{m_i\ v_i^2}{2}\right]_{Ek} \tag{2}$$

where m is the molar weight, F_z is the Faraday constant, g is the gravitational acceleration, h is the height, and v is the velocity. The terms in the brackets with the subscript $_{Ec}$ belong to energy due to the concentration of the solution, the terms with the subscript $_{Ef}$ belong to the fluid energy due to convection, the terms with the subscript $_{Ee}$ represent the energy contributed by an electromagnetic field, the terms with the subscript $_{Ep}$ correspond to the potential energy, and the terms with the subscript $_{Ek}$ belong to the fluid kinetic energy.

2.1. The Proposed Rotational Kinetic Energy PRO System

Figure 1 presents a schematic of a PRO system that includes a mechanism to generate an angular velocity ω. In said system, it is considered that there is no substantial external electromagnetic field and that there is not a substantial difference in the gravitational potential between the feed and draw solutions. With these considerations, the primary driving forces in the chemical potential equation are the chemical energy from concentration, the hydraulic pressure energy, and the kinetic energy associated with the angular velocity ω. With this, Equation (2) is

$$\mu_i = \left[\mu_i^0 + R\ T\ln\left(\frac{\gamma_i C_i}{\rho_i m_i}\right)\right]_{Ec} + [\hat{v}_i(P_i - P_{sati})]_{Ef} + \left[\frac{m_i\ v_i^2}{2}\right]_{Ek} \tag{3}$$

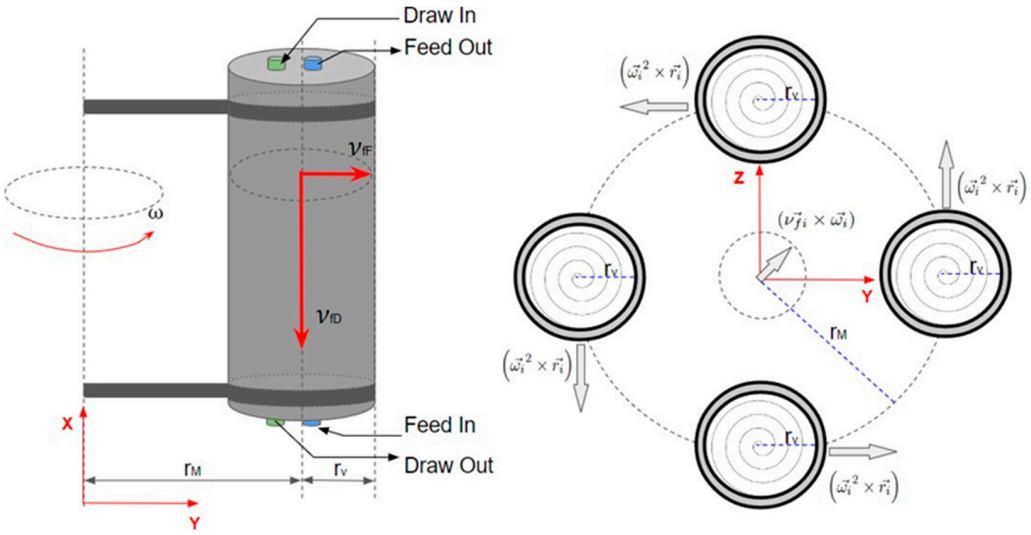


Figure 1. Schematic of a PRO system with an angular velocity.

The term that corresponds to kinetic energy has two components, a linear velocity v_{fi} that corresponds to the flow velocity produced by the applied pressure, and a component due to the angular velocity ω_i. The kinetic energy will be determined by the following equation:

$$E_k = \left[\frac{m_i \left(\vec{v}_{fi} + \vec{\omega}_i \times \vec{r} \right)^2}{2} \right] \tag{4}$$

If Equation (4) is expanded and simplified using some properties of scalar and vector product, the kinetic energy can be expressed as follows:

$$E_k = \left[\left(\frac{m_i \vec{v}_{fi}^{\,2}}{2} \right) + m_i \left(\vec{v}_{fi} \times \vec{\omega}_i \right) . \vec{r}_i + \left(\frac{\vec{\omega}_i^2 \times \left(m_i \vec{r}_i^{\,2} \right)}{2} \right) \right] \tag{5}$$

In Equation (5), the left-side term corresponds to the kinetic energy due to the fluid velocity generated by the applied hydraulic pressure, the central term corresponds to the kinetic energy due to Coriolis acceleration produced by the cross-product between the velocity of the fluid and the angular velocity, and the right side term corresponds to the rotational kinetic energy that is determined by the half of the cross-product of the square of the angular velocity with the moment of inertia of the rotational body. According to what has been previously described, Equation (3) can be written as follows:

$$\mu_i = \left[\mu_i^0 + R\ T\ ln\left(\frac{\gamma_i C_i}{\rho_i m_i} \right) \right]_{Ec} + \left[\hat{v}_i (P_i - P_{sati}) \right]_{Ef} + \left[\left(\frac{m_i \vec{v}_{fi}^{\,2}}{2} \right) + m_i (\vec{v}_{fi} \times \vec{\omega}_i) . \vec{r}_i + \left(\frac{\vec{\omega}_i^2 \times \left(\vec{I}_i \right)}{2} \right) \right]_{Ek} \tag{6}$$

where $\vec{I}_i = m_i . \vec{r}_i^{\,2}$ is the total moment of inertia. In the case of the system of Figure 1, the rotational axis does not go through the center of mass of the PRO module, and according to the Huygens–Steiner theorem, also known as the parallel axis theorem, we can describe the moment of inertia of the system as $I_{pa} = I_{cm} + m\ r^2$, where I_{cm} is the moment of inertia of an object when the rotational axis goes through the center of mass, plus the product of the total mass by the square of the perpendicular distance between the parallel axis. Considering the

PRO module as a straight circular cylinder with radius r_v and the perpendicular distance between the rotational axis and the cylinder's axis as r_M, the total moment of inertia is given by

$$\vec{I}_i = \frac{m_i.\left(r_v^2 + 2\,\vec{r}_M^{\,2}\right)}{2} \tag{7}$$

Replacing Equation (7) on Equation (6), we obtain the following:

$$\begin{aligned} l\mu_i = \left[\mu_i^0 + R\,T\ln\left(\frac{\gamma_i C_i}{\rho_i m_i}\right)\right]_{Ec} + [\hat{v}_i(P_i - P_{sati})]_{Ef} \\ + \left[\left(\frac{m_i \vec{v}_{fi}^{\,2}}{2}\right) + m_i\left(\vec{v}_{fi} \times \vec{\omega}_i\right).\vec{r}_i \right. \\ \left. + \left(\frac{\vec{\omega}_i^2 \times m_i.\left(0.5\vec{r}_v^2 + \vec{r}_M^2\right)}{2}\right)\right]_{Ek} \end{aligned} \tag{8}$$

As per the scheme in Figure 1, it is considered a PRO system with a spiral-wound planar membrane, on which the feed and draw solutions are in a counter-flow configuration. The membrane's spiral geometry lies in the ZY plane (See Figure 2), and only the potentials acting within this plane are considered to directly affect diffusion through the membrane.

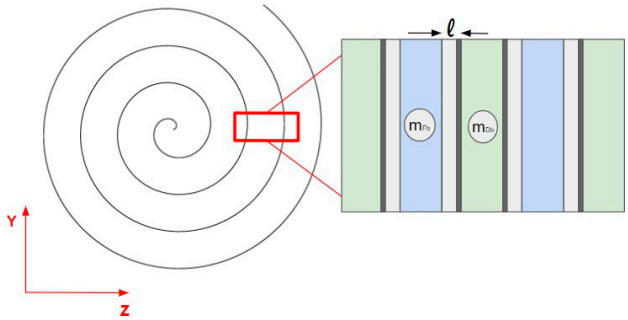


Figure 2. Scheme of the ZY plane of the spiral-wound membrane considered for a PRO process.

2.2. Draw Solution Energy Balance

For the draw solution, the main component of the draw fluid's velocity, v_{fD} is due to the applied hydraulic pressure and goes in the negative direction of the x-axis. This velocity runs parallel to the membrane surface, so its contribution to diffusive transport through the membrane is considered minimal. However, if the flow is turbulent, the components v_{fD} (0, j, k) could enhance diffusion through the membrane. This turbulence can also help refresh concentration levels near the membrane, which may decrease due to solvent diffusion.

Now, considering that the system is rotating around the x-axis with an angular velocity ω_D (i, 0, 0) and that the turning radius for the system will be inside the YZ-plane, the vector product of the square of the angular velocity and the radius is on the YZ-plane and is going to contribute directly to the diffusion.

The component of the kinetic energy related to the Coriolis acceleration depends on the vector product between the fluid's velocity v_{fD} ($-i$, 0, 0) and the angular velocity ω_D (i, 0, 0), and for this reason, it will be 0.

With these considerations, the draw solution chemical potential on the Z axis is

$$\mu_D = \left[\mu_D^0 + R\,T\ln\left(\frac{\gamma_D C_D}{\rho_D m_D}\right)\right]_{Ec} + [\hat{v_D}(P_D - P_{sat,D})]_{Ef} + \left[\left(\frac{\vec{\omega}_D^2 \times \vec{I}_D}{2}\right)\right]_{Ek} \tag{9}$$

Considering Figure A1 again, we can propose an energy difference between the chemical potential of the bulk draw solution (μ_{Db}) and of the area near the membrane (μ_{Dm}). Even though there can be differences between the velocities, concentrations, or pressures between the bulk of the solutions and the area near the membrane, by being a lossless closed system, the internal energies should remain equal. We propose the equation $\mu_{Db} = \mu_{Dm}$.

$$\begin{aligned} \mu_D^0 + R\ T \ln\left(\frac{\gamma_{Db}\ C_{Db}}{\rho_{Db}\ m_{Db}}\right) + \hat{v}_{Db}(P_{Db} - P_{sat,Db}) + \left(\frac{\vec{\omega}_{Db}^2 \times \vec{I}_{Db}}{2}\right) = \mu_D^0 \\ + R.T.\ln\left(\frac{\gamma_{Dm}\ C_{Dm}}{\rho_{Dm}\ m_{Dm}}\right) + \hat{v}_{Dm}(P_{Dm} - P_{sat,Dm}) + \left(\frac{\vec{\omega}_{Dm}^2 \times \vec{I}_{Dm}}{2}\right) \end{aligned} \tag{10}$$

From Equation (10), if it is considered that water is an incompressible liquid and that the membrane is a solid and dense element, we can consider ($P_{Db} = P_{Dm}$, $\hat{v}_{Db} = \hat{v}_{Dm}$), and with this, we arrive at the following expression:

$$C_{Dm} = C_{Db}\ G_D\ e^{\left[\frac{1}{2\ R\ T}.(\omega_{Db}^2 \times I_{Db} - \omega_{Dm}^2 \times I_{Dm})\right]} \tag{11}$$

where

$$G_D = \frac{\gamma_{Db}\ \rho_{Dm}}{\gamma_{Dm}\ \rho_{Db}}$$

2.2.1. Feed Solution Energy Balance

For the feed solution, it is necessary to consider that the main component of the fluid's velocity v_{fF}, due to the spiral-wound module geometry, which varies its direction inside the ZY-plane (0, j, k) parallel to the membrane surface. Even though components of this velocity could affect diffusion through the membrane, as the feed solution flow velocity is usually small, this contribution will be neglected. Now, concerning the rotational motion, just as in the draw solution, the vector product of the square of the angular velocity and the radius will be on the Z axis and will contribute directly to diffusion through the membrane.

The Coriolis acceleration results of the vector product of the flow velocity v_{fF} (0, j, k) and angular velocity ω_F (i, 0, 0), because of this, will alternate between zero and a maximum value in the Y or Z axis, respectively, and will contribute to diffusion through the membrane.

In the vector product for Coriolis energy, the angular velocity ω appears in the second position, unlike in the vector product for centrifugal energy, where it occupies the first position. As a result, when $\vec{v}_{fF}$ is aligned with $\vec{r}_M$, the Coriolis energy will have the opposite direction to the centrifugal energy.

For ease in handling the equations, we will call the Coriolis energy as follows:

$$Cor_i = m_i\left(\vec{v}_{fi} \times \vec{\omega}_i\right).\vec{r}_i$$

With these considerations, the energy balance for the Feed solution will be $\mu_{Fm} = \mu_{Fb}$.

$$\begin{aligned} \mu_F^0 + R\ T \ln\left(\frac{\gamma_{Fm}\ C_{Fm}}{\rho_{Fm}\ m_{Fm}}\right) + \hat{v}_{Fm}(P_{Fm} - P_{sat,Fm}) + \left(\frac{\vec{\omega}_{Fm}^2 \times \vec{I}_{Fm}}{2} + Cor_{Fm}\right) = \mu_F^0 + \\ R\ T \ln\left(\frac{\gamma_{Fb}\ C_{Fb}}{\rho_{Fb}\ m_{Fb}}\right) + \hat{v}_{Fb}(P_{Fb} - P_{sat,Fb}) + \left(\frac{\vec{\omega}_{Fb}^2 \times \vec{I}_{Fb}}{2} + Cor_{Fb}\right) \end{aligned} \tag{12}$$

In this case, additionally, from the considerations related to the volumes and the incompressibility of the solution, it is considered that $P_{Fm} = P_{Db}$, and after simplifying Equation (12), we arrive at the following equation:

$$C_{Fm} = C_{Fb}\, G_F\, e^{\left[\frac{1}{2RT}.(\omega_{Fb}^2 \times I_{Fb} + 2Cor_{Fb} - \omega_{Fm}^2 \times I_{Fm} - 2Cor_{Fm}) - \frac{\vec{v}_F}{RT}(P_{Db} - P_{Fb})\right]} \tag{13}$$

where

$$G_F = \frac{\gamma_{Fb}\, \rho_{Fm}}{\gamma_{Fm}\, \rho_{Fb}}$$

If we consider a semipermeable membrane, as shown in Figure A1, and assume a solvent flux primarily driven by diffusion, applying Fick's law leads to the following expression:

$$J_w = \frac{D_w}{l}(C_{Dm} - C_{Fm}) \tag{14}$$

When we replace Equations (11) and (13) in Equation (14),

$$\begin{aligned} &J_w \\ &= \tfrac{D_w}{l}\Bigg(C_{Db}\, G_D\, e^{\left[\frac{1}{2\,R\,T}.(\omega_{Db}^2 \times I_{Db} - \omega_{Dm}^2 \times I_{Dm}) - \frac{\vec{v}_F}{RT}(P_{Db} - P_{Fb})\right]} \\ &- C_{Fm}\, G_F\, e^{\left[\frac{1}{2\,R\,T}.(\omega_{Fb}^2 \times I_{Fb} + 2Cor_{Fb} - \omega_{Fm}^2 \times I_{Fm} - 2Cor_{Fm}) - \frac{\vec{v}_F}{RT}(P_{Db} - P_{Fb})\right]}\Bigg) \end{aligned} \tag{15}$$

2.2.2. Equilibrium Point

In osmotic processes, a key point of interest is where the driving forces balance, causing the solvent flow to stop. In the scenario shown in Figure 1, with zero flow in both the draw and feed solutions, an equilibrium in kinetic energy is established, satisfying the condition $\Delta E_{RKE} = 0$ for both the draw and feed solutions and between them.

$$\begin{aligned} \omega_{Db}^2 \times I_{Db} = \quad & \omega_{Dm}^2 \times I_{Dm} \\ = \quad & \omega_{Fb}^2 \times I_{Fb} \\ = \quad & \omega_{Fm}^2 \times I_{Fm} \\ = \quad & 2.m_{Fb}.\left(\vec{v}_{f,Fb} \times \vec{\omega}_{Fb}\right).\vec{r}_{Fb} \\ = \quad & 2.m_{Fm}.\left(\vec{v}_{f,Fm} \times \vec{\omega}_{Fm}\right).\vec{r}_{Fm} \end{aligned} \tag{16}$$

Additionally, this working point will be defined by the equilibrium between the osmotic potential, the hydraulic pressure potential, and the kinetic energy potential ($\Delta\Pi + \Delta P + \Delta P_{RKE} = 0$). Taking into account that $\Delta P_{RKE} = 0$, then $\Delta\Pi = \Delta P$. Evaluating these considerations in Equation (15), we arrive at the following:

$$C_{Fb} = C_{Db}\frac{G_D}{G_F}e^{\frac{\hat{v}_F}{RT}\Delta\Pi} \tag{17}$$

2.3. The Proposed Solution–Diffusion Model with Rotational Kinetic Energy

Equation (17) relates the bulk concentration of the feed solution with the bulk concentration of the draw solution.

When substituting Equation (17) into Equation (15) and reorganizing, we obtain the following:

$$\begin{aligned} J_w = \tfrac{D_w\, C_{Db}\, G_D}{l}\Bigg(&e^{\left[\frac{1}{2\,R\,T}.(\omega_{Db}^2 \times I_{Db} - \omega_{Dm}^2 \times I_{Dm})\right]} - \\ &e^{\left[\frac{1}{2\,R\,T}.(\omega_{Fb}^2 \times I_{Fb} + 2Cor_{Fb} - \omega_{Fm}^2 \times I_{Fm} - 2Cor_{Fm}) - \frac{\vec{v}_F}{RT}(P_{Db} - P_{Fb}) + \frac{\vec{v}_F}{RT}\Delta\Pi\right]}\Bigg) \end{aligned} \tag{18}$$

If, in Equation (18), we consider the exponential function definition ($e^x \approx 1 + x$ for $-1 < x < 1$),

$$J_w = \frac{D_w\, C_{Db}\, G_D}{lRT}\left(\left[1 + \tfrac{1}{2}\left(\omega_{Db}^2 \times I_{Db} - \omega_{Dm}^2 \times I_{Dm}\right]\right) - \left[1 + \tfrac{1}{2}\left(\omega_{Fb}^2 \times I_{Fb} + 2Cor_{Fb} - \omega_{Fm}^2 \times I_{Fm} - 2Cor_{Fm}\right) - \vec{\nu}_F(P_{Db} - P_{Fb}) + \vec{\nu}_F\, \Delta\Pi\right]\right) \tag{19}$$

In Equation (19), we must consider that, due to the flux through the membrane, the kinetic energy in the area near the membrane will be equal for the feed and draw solutions. Due to this, $\omega^2 \times I_{Dm} = \omega^2 \times I_{Fm} + 2\, Cor_{Fm}$. After simplifying the expression, we obtain the following:

$$J_w = \frac{D_w\, C_{Db}\, G_D}{l\, R\, T}\left(\vec{\nu}_F\, \Delta\Pi - \vec{\nu}_F(P_{Db} - P_{Fb}) - \frac{1}{2}\left[\omega_{Db}^2 \times I_{Db} - \omega_{Fb}^2 \times I_{Fb} - 2Cor_{Fb}\right]\right) \tag{20}$$

Now, substituting Equation (7) in Equation (20) and writing the molar mass m_i in terms of the molar density ρ_i and the molar volume $\hat{v}_i$,

$$\begin{aligned} J_w = -\frac{D_w\, C_{Db}\, G_D}{l\, R\, T}\Big(&\hat{v}_F\, \Delta\Pi - \hat{v}_F(P_{Db} - P_{Fb}) \\ &-\hat{v}_F \tfrac{1}{2}\left[\omega_{Db}^2 \times \rho_{Db}\left(0.5\vec{r}^{\,2}_{v,Db} + \vec{r}^{\,2}_{M,Db}\right)\right. \\ &\left.-\omega_{Fb}^2 \times \rho_{Fb}\left(0.5\vec{r}^{\,2}_{v,Fb} + \vec{r}^{\,2}_{M,Fb}\right)\right] \\ &+\hat{v}_F\left[\rho_{Fb}\vec{\nu}_{f,Fb} \times \vec{\omega}_{Fb}.\vec{r}_{MFb}\right]\Big) \end{aligned} \tag{21}$$

Finally, considering that the difference between the flow velocity, angular velocity, and the radius of the bulk of the feed and draw solutions is very small, Equation (21) can be written in a compact form as

$$J_w = A\,(\Delta\Pi - \Delta P - \Delta P_{RKE}) \tag{22}$$

where

$$A = -\frac{D_w C_{Db} G_D \hat{v}_F}{lRT}$$

$$\Delta\Pi = iRT(C_{Db} - C_{Fb})$$

$$\Delta P = (P_{Db} - P_{Fb})$$

$$\Delta P_{RKE} = 0.5\left(\omega_{Db}^2 \times \left(0.5\vec{r}^{\,2}_{v,Db} + \vec{r}^{\,2}_{M,Db}\right)\right)(\rho_{Db} - \rho_{Fb}) - \left(\rho_{Fb}\vec{\nu}_{f,Fb} \times \vec{\omega}_{Fb}.\vec{r}_{MFb}\right)$$

Equation (22) describes a process where diffusion through the semipermeable membrane is driven by the potential differences of three types of energy: chemical energy, represented by the osmotic potential $\Delta\Pi$; convective energy, arising from the applied hydraulic pressure ΔP; and rotational kinetic energy, represented by the dynamic pressure ΔP_{RKE}.

The term ΔP_{RKE} indicates that the equivalent hydraulic pressure exerted on the membrane by rotational kinetic energy is determined by the angular velocity ω, the total radius that will be simplified as r_M, the fluid velocity of the draw solution $v_{\vec{f}}$, and the densities of the feed and draw solutions, which depend on their concentrations. While the channel heights for the feed and draw solutions could also influence the resulting pressure, this effect is beyond the scope of this study.

Depending on the directions of vectors $\vec{\omega}$, $\vec{\nu}$, and $\vec{r}$, within the spiral membrane module, the resultant dynamic pressure Δ_{RKE} can either support or oppose the osmotic pressure $\Delta\Pi$. However, the local hydrodynamic effects on the membrane surface can help

mitigate the negative impacts of concentration polarization CP or membrane fouling in real time. These overall positive effects suggest that further research into this technology is well justified.

Although some studies have explored the use of rotational kinetic energy to modify flow through membranes in osmotic processes like RO, to the best of the authors' knowledge, this is the first analytical model to explicitly incorporate rotational kinetic energy in PRO.

3. Results and Discussion

As shown in Equation (22), the effects of rotational kinetic energy depend on the densities of the feed and draw solutions, which vary with concentration due to phenomena such as ICP, CECP, and DECP. By calculating these densities numerically or using mathematical models that account for these effects, it would be possible to couple the system equations and simulate the impact of rotational kinetic energy on these phenomena. Figure 3 illustrates the concentration variations across the bulk and membrane regions in both the active and support layers. The effective osmotic pressure, considering the impact of ICP, is expressed as $\Delta\Pi = C_2 - C_3$ and will be simulated using Equation (23) from [17].

$$C_3 = \frac{C_2\left[B\left(e^{(J_w.K)} - 1\right) + J_w\frac{C_4}{C_2}e^{(J_w.K)}\right]}{B\left(e^{(J_w.K)} - 1\right) + J_w} \quad (23)$$

To verify the analytical model behavior under typical PRO conditions, Equations (22) and (23), with the parameters in Table 1, are used to simulate the PRO system with rotational kinetic energy. The concentrations of the feed and draw solutions are used with a library developed by [18] for Engineering Equation solver (EES) software, version 10.834-3D, to calculate the values for the osmotic pressure and the densities.

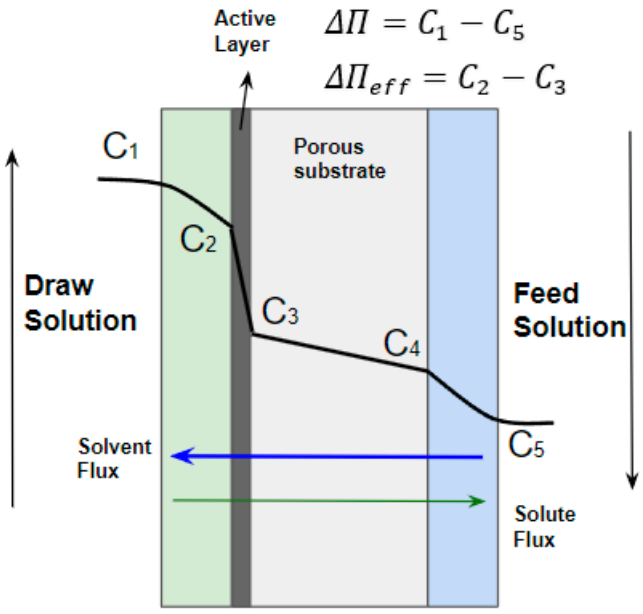


Figure 3. Schematic of the different concentrations related to a membrane in osmotic processes. Modified from [17].

Table 1. PRO with rotational kinetic energy mechanism characteristics, membrane characteristics, and operating conditions for the simulation [19].

Parameter	Value
Mechanism radius (r_M)	0.5 m
Angular velocity (ω)	0–2700 rev/min
Membrane water permeability (A)	1.763×10^{-12} [m/s Pa]
Membrane solute permeability (B)	1.17×10^{-7} [m/s]
Solute resistivity (K)	3.38×10^{5} [s/m]
Temperature (T)	25 [°C]
Atmospheric pressure (P)	0.101325 [MPa]
Draw solution concentration (C_2)	35 g/kg
Draw solution flow rate (Q_{fD})	22.5 L/min
Feed solution concentration (C_5)	0.584 g/kg
Feed solution flow rate (Q_{fF})	7 L/min

3.1. Compensating for ICP Losses

In this section, we compare the performance of three versions of the solution–diffusion model: the ideal model, a model that considers ICP, and a model that considers ICP plus rotational kinetic energy. As we are not considering the effects of other phenomena like external concentration polarization (ECP), the simulated values obtained for water flow and power density are overestimated when compared with experimental results in spiral-wound modules from works like [19,20], but it is considered that the results are coherent for the simulated conditions.

Figure 4 shows how increasing the angular velocity ω for the system under ICP conditions increments its water flow to match the ideal model water flow. For this simulation, ΔP is set to reach the ideal maximum power for the given concentration. For a PRO system working near the maximum power operating point, it would be possible to actively compensate for water flow losses over time that are intrinsic to PRO operation.

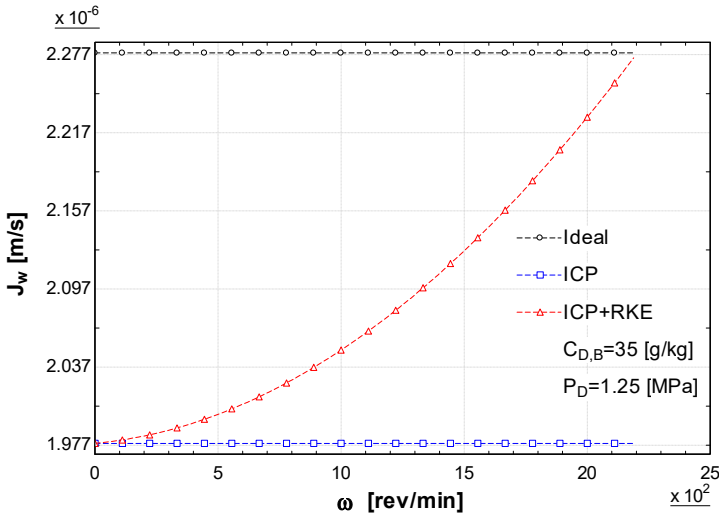


Figure 4. Change in water flow with variations in angular velocity.

Figure 5 presents the required angular velocity needed to compensate for ICP losses with a fixed concentration difference of approximately 35 g/kg for different values of draw solution concentration. From these results, it could be inferred that even if the $\Delta\Pi$ is the same, for higher concentrations of the feed and draw solutions, the angular velocity needed to compensate for the water flow losses will increase in a non-linear fashion.

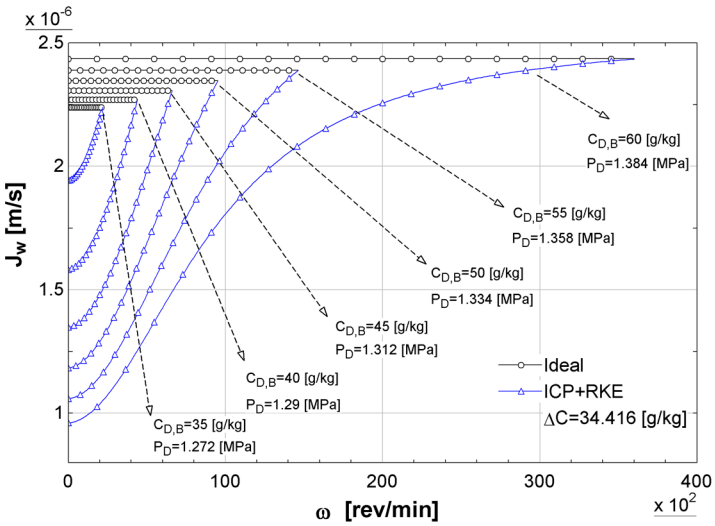


Figure 5. ICP losses compensated for different draw solution concentrations and a fixed concentration difference.

Figure 6 illustrates how ICP losses can be compensated for various ΔΠ values. The results indicate that the angular velocity ω does not increase significantly, even when ΔΠ is doubled. Since the theoretical extractable energy rises with ΔΠ, this suggests that in a PRO system utilizing rotational kinetic energy, the net available energy—after accounting for ICP losses—will be higher for greater ΔΠ values. In other words, the proportion of rotational kinetic energy required to offset ICP losses will decrease as the salinity gradient increases.

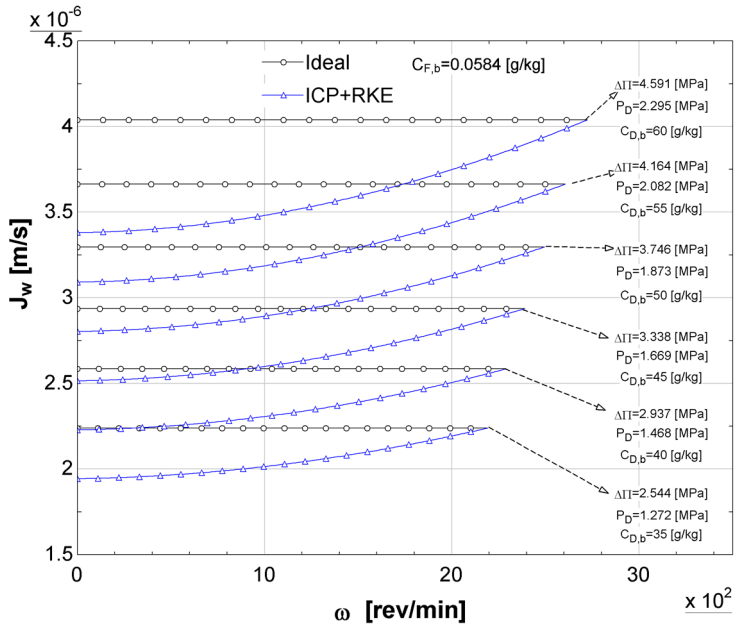


Figure 6. ICP losses compensated for some concentration differences.

Figure 7 shows the water flow under variations of the applied hydraulic pressure P_D. A fixed value of ω was used to bring the system from ICP levels to the ideal model level. Similarly, Figure 8 presents the power density variation for the three models due to variation in the applied P_D.

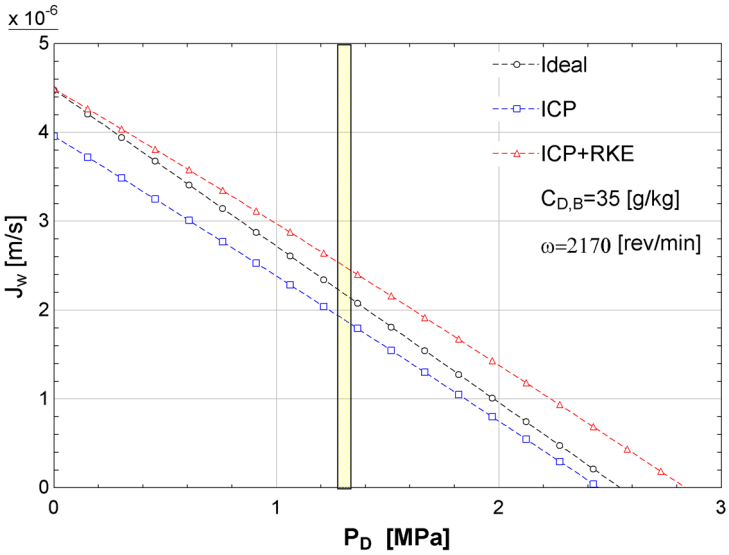


Figure 7. ICP waterflow losses compensated for by a fixed angular velocity with variations in applied *PD*. The yellow area indicates half of the osmotic pressure.

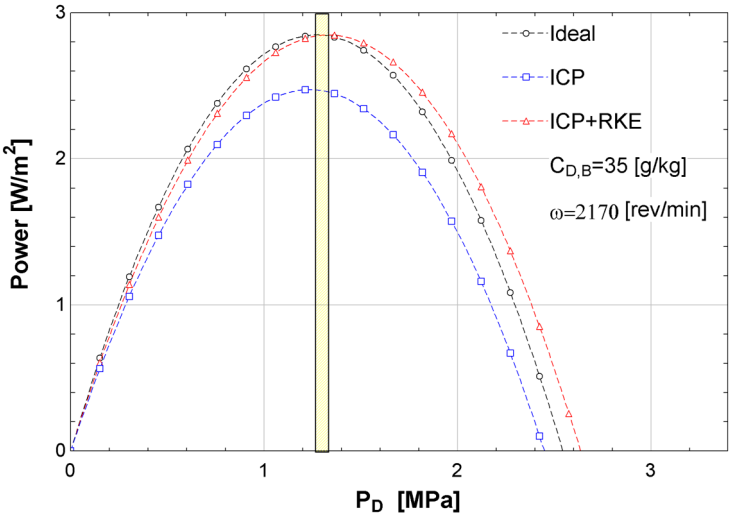


Figure 8. Power density compensated for by rotational kinetic energy. The yellow area indicates half of the osmotic pressure.

3.2. Dynamic Pressure Components

The dynamic pressure generated by rotational kinetic energy consists of two main components: the centrifugal and Coriolis forces. These components, governed by distinct physical principles and equations, respond differently to the operational parameters of a PRO system.

Figure 9 presents the variations in centrifugal pressure for different draw solution concentrations as the angular velocity ω changes. As the draw solution concentration increases, the influence of ω on centrifugal pressure becomes more pronounced, requiring lower angular velocities to achieve a given pressure. Higher-concentration draw solutions provide a greater salinity gradient, leading to higher theoretical energy generation. However, in PRO systems, the effects of ICP are more severe with higher-concentration solutions, significantly reducing the available energy. While utilizing rotational kinetic energy to mitigate ICP consumes electrical energy, its efficient application could potentially enhance power density in PRO systems.

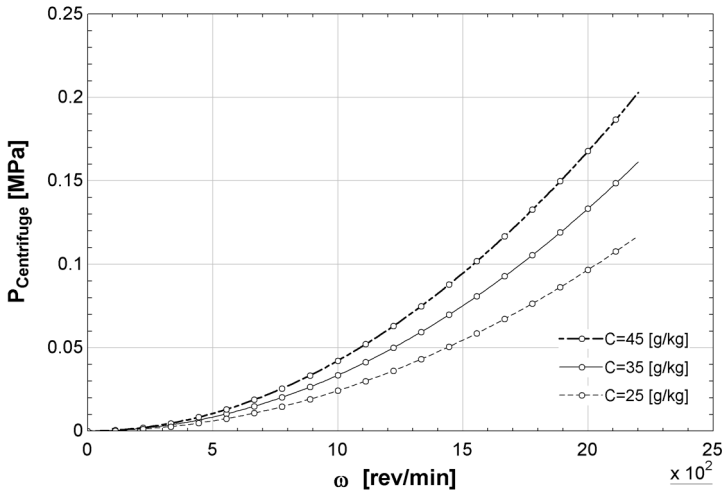


Figure 9. Change in centrifuge-generated dynamic pressure with changes in draw solution concentration.

Regarding the Coriolis pressure component, the solution–diffusion model, which incorporates ICP and rotational kinetic energy, reveals that due to the differing paths of the feed and draw solutions in the spiral-wound modules of the PRO system, the Coriolis forces act in opposite directions and do not cancel each other out. As a result, the Coriolis pressure is primarily influenced by the flow velocity $\vec{v}$ and is not affected by the draw solution concentration. Figure 10 illustrates this behavior.

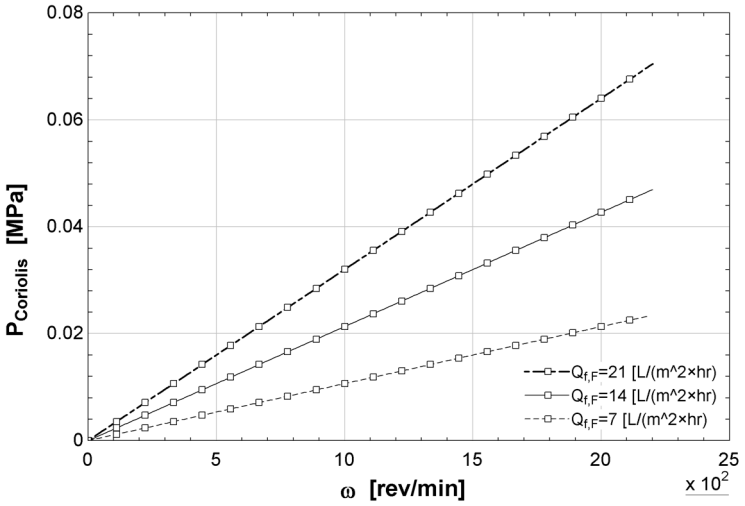


Figure 10. Change in Coriolis-generated dynamic pressure with changes in feed solution volumetric flow.

4. Conclusions

This research presents an analytical mathematical model, providing a theoretical framework grounded in fundamental principles that can be universally applied under the specified conditions. It was developed systematically, beginning with the chemical potential equation for a solution, incorporating the additional forces considered, and integrating these with Fick's law to capture the influence of kinetic energy on diffusion through the membrane. The model emphasizes mathematical rigor while incorporating key simplifications, making it a practical tool accessible to individuals with an engineering background. Based on the simulation results, the primary findings can be summarized as follows.

The developed analytical model offers a framework to include other impulse forces in osmotic processes, as the used methodology could be replicated considering other external forces.

Equation (22) could be combined with other solution–diffusion models that consider other forms of CP or membrane fouling to obtain a more precise analytical model for rotational kinetic energy under the considerations made in the present work, which can actively control the negative effects caused by ICP.

The length (0.5 (m)) and the angular velocity (0–3000 (rev/min)) of the mechanism needed to implement rotational kinetic energy could be implemented with simple commercially available components.

The developed model incorporates the control of internal concentration polarization (ICP) through rotational kinetic energy, addressing a key challenge in the commercialization of PRO. It also provides an energy balance method, and we verified the model through simulations based on the existing literature.

Our findings suggest that optimized turning radius and angular speed can compensate for ICP losses, improving the efficiency of PRO. Furthermore, the results highlight the benefits of larger concentration differences for energy extraction.

Future research work should be oriented to address the technical difficulties of the implementation of the proposed PRO system.

Author Contributions: D.R.-N.: investigation, data curation, modeling, writing—original draft. E.Q.-B.: data curation, writing—original draft. M.H.S.: conceptualization, methodology, supervision, writing—review and editing. All authors have read and agreed to the published version of the manuscript.

Funding: This research was co-funded by the Natural Sciences and Engineering Research Council of Canada (NSERC–Grant #401366) and the Research Vice Presidency of the University of Cartagena, initiation and commitment record No. 021-2022—Resolution 01880 of 2022.

Institutional Review Board Statement: Not applicable.

Informed Consent Statement: Not applicable.

Data Availability Statement: Data will be made available on request.

Conflicts of Interest: The authors declare no conflicts of interest. The authors declare that they have no known competing financial interests or personal relationships that could have appeared to influence the work reported in this paper.

Nomenclature

Symbol	Description	Units
ΔP	hydraulic pressure differential	Pa
$\Delta\Pi$	osmotic pressure differential	Pa
γ	activity coefficient	-
μ	chemical potential of a solution	J/mol
ν	velocity	m/s
ω	angular velocity of the rotation mechanism for PRO	rad/s
ρ	molarity	mol/m^3
$\hat{v}$	molar volume	m^3/mol
A	water permeability	m/s Pa
a	activity of a component in a solution	-
B	solute permeability	m/s
C	concentration	g/kg
D	diffusion coefficient	m^2/s

E	electrical potential	J/C
F_z	Faraday constant 9.648×10^4	C/mol
G	constant in Equations (A3) and (A5)	-
g	gravitational acceleration	m/s^2
h	height	m
I	total moment of inertia	$kg.m^2$
J	solvent flow	m/s
K	solute resistivity	s/m
k	mass transfer coefficient	m/s
l	length of the of the membrane	m
M	molecular weight	g/mol
P	pressure	Pa
Q	volumetric flowrate	L/min
R	gas constant (8.314462)	J/(K mol)
r	radius of rotation	m
T	temperature	K

Subscripts

Symbol	Description
b	zone in the bulk of the solution
D	draw solution
d	dynamic component
F	feed solution
f	flow
i	the i-th element in a solution
M	rotating mechanism
m	zone near the membrane
RKE	rotational kinetic energy
sat	saturation vapor pressure
s	static component
v	pressure vessel
w	water

Superscripts

Symbol	Description
0	property of a pure element

Acronyms

Symbol	Description
2RO-DSPRO	two-pass reverse osmosis with dual-stage pressure-retarded osmosis
AL-DS	active layer draw side
AL-FS	active layer feed side
CECP	concentrative external concentration polarization
CICP	concentrative internal concentration polarization
CMS	centrifugal membrane separation
CP	concentration polarization
CRO	centrifugal reverse osmosis
DECP	dilutive external concentration polarization
ECP	external concentration polarization
ICP	internal concentration polarization
PRO	pressure-retarded osmosis
RO	reverse osmosis
RSF	reverse solute flux

Appendix A

Appendix A.1. Analytical Method for Obtaining the Solution–Diffusion Model

In [21], the authors use an energy balance method and Fick's law to obtain the solution–diffusion model. The authors consider that the chemical potential of the *i*-th element in a solution μ_i mainly comprises a concentration component and a convective component.

$$\mu_i = \mu_i^0 + R\ T\ ln\left(\frac{\gamma_i\ C_i}{\rho_i\ m_i}\right) + \hat{v}\ (P_i - P_{sat,i}) \tag{A1}$$

where R is the gas constant, T is the temperature, γ is the activity coefficient, C is the concentration, M is the molecular weight, ρ is the molecular density, $\hat{v}$ is the molar volume, and P is pressure. The superscript 0 denotes that the quantity corresponds to a pure substance, the subscript i denotes the i-th element in a solution, and the subscript *sat* refers to the saturation vapor pressure.

Figure A1 shows a membrane in an osmotic process. It shows the parameters necessary to establish a difference between the chemical potential of the bulk of the feed and draw solutions (μ_{Db} and μ_{Fb}) and the chemical potential on the area near the membrane (μ_{Dm} and μ_{Fm}).

Now, for the draw solution side, regarding the velocities, concentrations, and pressures between the bulk of the feed and draw solutions and these parameters in the area near the membrane, considering a closed system that has no losses, the chemical potential should remain balanced. We have, then, the following equation: $\mu_{Db} = \mu_{Dm}$.

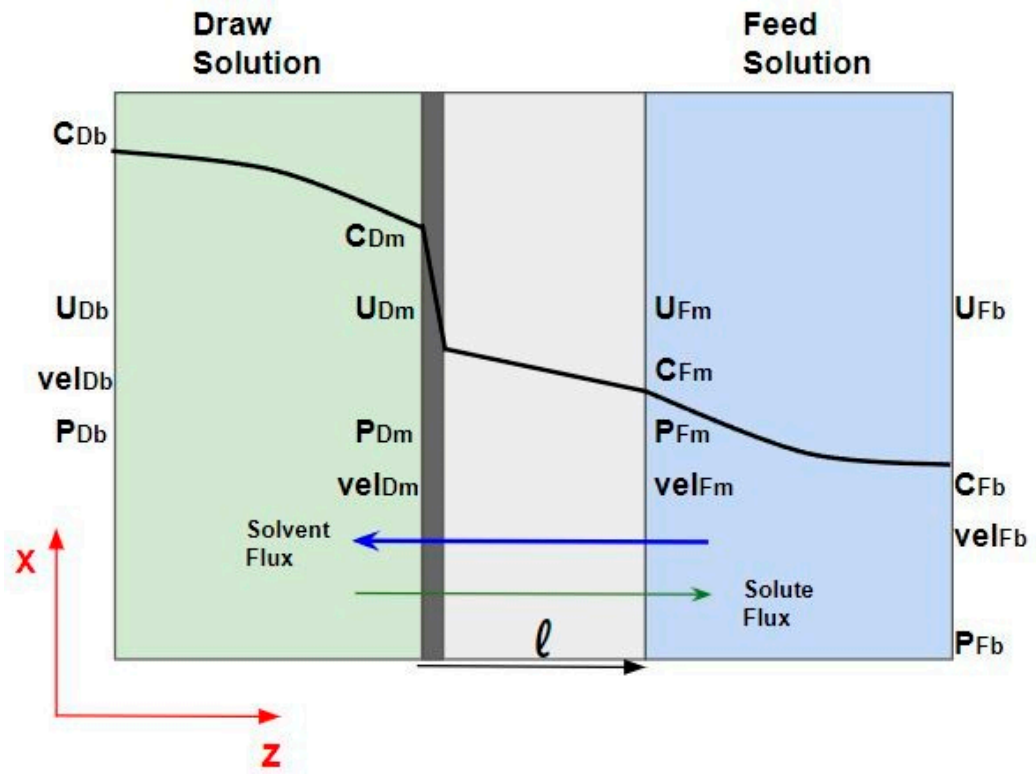


Figure A1. Schematic of the chemical potential components in an osmotic process.

$$\mu_D^0 + R\ T\ ln\left(\frac{\gamma_{Db}C_{Db}}{\rho_{Db}m_{Db}}\right) + \hat{v}_{Db}(P_{Db} - P_{sat,Db}) = \mu_D^0 + R\ T\ ln\left(\frac{\gamma_{Dm}C_{Dm}}{\rho_{Dm}m_{Dm}}\right) + \hat{v}_{Dm}(P_{Dm} - P_{sat,Dm}) \tag{A2}$$

where subscripts D and F correspond to quantities in the draw and feed solution, and the subscripts b and m correspond to the zone near the membrane and the zone.

From Equation (A2), when considering that the water is an incompressible fluid and that the membrane is a solid dense element ($P_{Db} = P_{Dm}$, $\hat{v}_{Db} = \hat{v}_{Dm}$), we arrive at the following expression:

$$C_{Dm} = C_{Db}\, G_D \tag{A3}$$

where the auxiliary variable G_D is defined as follows:

$$G_D = \frac{\gamma_{Db}\, C_{Fb}}{\gamma_{Dm}\, C_{Db}}$$

Similarly, when we perform an energy balance at the feed solution, we have the following: $\mu_{Fm} = \mu Fb$.

$$\mu_{\mathrm{F}}^{0} + R\ T \ln\left(\frac{\gamma_{\mathrm{Fb}} C_{\mathrm{Fb}}}{\rho_{\mathrm{Fb}} m_{\mathrm{Fb}}}\right) + \hat{v}_{Fb}(P_{\mathrm{Fb}} - P_{sat,Fb}) = \mu_{\mathrm{F}}^{0} + R\ T \ln\left(\frac{\gamma_{\mathrm{Fm}} C_{\mathrm{Fm}}}{\rho_{\mathrm{Fm}} m_{Fm}}\right) + \hat{v}_{Fm}(P_{\mathrm{Fm}} - P_{sat,\mathrm{Fm}}) \tag{A4}$$

In this case, in addition to the considerations related to volumes and liquid incompressibility, we consider that $P_{Fm} = P_{Db}$, and after rearranging expression (A4), we obtain the following equation:

$$\mathrm{C_{Fm}} = \mathrm{C_{Fb}}\ \mathrm{G_F}\ e^{-\frac{\hat{v}_F}{RT}(P_{Db} - P_{Fb})} \tag{A5}$$

where the auxiliary variable G_F is defined as follows:

$$G_D = \frac{\gamma_{Db}\, C_{Fb}}{\gamma_{Dm}\, C_{Db}}$$

We have, then, a semipermeable membrane like the one presented in Figure A1. If it is considered that the solvent flow on its majority is due to the diffusive effect, we make use of Fick's law and arrive at the following expression:

$$J_w = \frac{D_w}{l}(C_{Dm} - C_{Fm}) \tag{A6}$$

where l is the length of the cross-section of the membrane, and D_w is the diffusivity of the water. When we replace Equations (A3) and (A5) in Equation (A6), we obtain the following:

$$J_w = \frac{D_w}{l}\left(C_{Db}\ G_D - C_{Fb}\ G_F\ e^{\frac{\hat{v}_F}{RT}(P_{Db} - P_{Fb})}\right) \tag{A7}$$

Up to this point, we have considered a generic osmotic process. If in Equation (A7), we consider the point of interest when the pressure potentials match each other ($\Delta\Pi = \Delta P$) and the solvent flux becomes zero ($J = 0$),

$$\mathrm{C_{Fb}} = \mathrm{C_{Db}}\ \frac{\mathrm{G_D}}{G_F}\ e^{\frac{\hat{v}_F}{RT}(\Delta\Pi)} \tag{A8}$$

If we replace Equation (A8) in Equation (A7) and simplify, we arrive at

$$J_w = \frac{D_w\ C_{Db}\ G_D}{l}\left(1 - e^{\frac{\hat{v}_F}{RT}(\Delta\Pi - P_{Db} + P_{Fb})}\right) \tag{A9}$$

Now, if in Equation (A9), we consider the definition of an exponential function ($ex \approx 1 + x$ for $-1 < x < 1$), we could write

$$J_w = \frac{D_w\ C_{Db}\ G_D\ \hat{v}_F}{lRT}(\Delta\Pi - P_{Db} + P_{Fb}) \tag{A10}$$

Finally, Equation (A10) can be written as

$$J_w = A(\Delta\Pi - \Delta P) \tag{A11}$$

where

$$\begin{aligned} A &= \frac{D_w\, C_{Db}\, G_D\, \hat{v}_F}{lRT} \\ \Delta\Pi &= (C_{Dm} - C_{Fm}) \\ \Delta P &= (P_{Db} - P_{Fb}) \end{aligned} \tag{A12}$$

Equation (A11) is the equation that describes the solution–diffusion model that has been traditionally used in osmotic processes.

Appendix A.2. Short Review on Research Work with Solution–Diffusion-Based Models

Table A1. Some of the most representative mathematical models for pressure-retarded osmosis over the years.

Reference	Objective	Osmotic Process	Type of Membrane
[22]	Considers the asymmetry between the semipermeable membrane and the porous support structure.	PRO	Hollow Fiber
[23]	Considers a more general case where the net flux in the transition zone due to the concentration in the support layer is nonzero.	PRO	Hollow Fiber
[24]	Proposes a two-parameter water transport equation to represent the permeation due to osmotic pressure and the permeation due to applied pressure on the high-concentration side.	PRO	Hollow Fiber
[7]	Defines the effective osmotic pressure by considering internal concentration polarization. They propose a simplified model when the feed is distilled water.	PRO	Flat Sheet
[25,26]	Conducts studies exploring the effects of internal concentration polarization (ICP) and external concentration polarization (ECP). They explore the effects of membrane orientation AL-FS and AL-DS.	PRO, FO	Flat Sheet
[27]	Presents an equation for the water flux that includes terms for external concentration polarization of dilution (DECP) and internal concentration polarization of concentration (CICP). In this equation, all terms can be measured or calculated, and it was validated with experimental results.	PRO	Flat Sheet
[28]	Suggests that the volumetric and solute permeability coefficients, A and B, along with the parameter S, can describe the osmotic efficiency of a membrane. Equation system to simulate PRO module	PRO	Flat Sheet
[29]	Presents expressions for the water flux are presented as a logarithmic function, directly proportional to the mass transfer factor in the porous substrate. They include an expression to calculate the concentration at any point in a modified spiral-wound module for PRO.	PRO	Flat Sheet

Table A1. *Cont.*

Reference	Objective	Osmotic Process	Type of Membrane
[30]	Includes in their mathematical analysis a transition zone to characterize the impact of DECP. They include the effects of CICP, DECP, and reverse salt flux.	PRO	Flat sheet
[31]	Uses cylindrical coordinates in their model to facilitate the understanding of variations in system behavior due to geometry.	PRO	Hollow Fiber
[32]	Expressions for the water flux in logarithmic form are provided for the configurations (AL-DS) and (AL-FS). Both equations consider the parameters A and B as constants; however, these can change under the effects of deformations caused by operating parameters.	PRO	Flat Sheet
[33]	Analyses the influence of spacers on the performance of PRO. They define the term "shadow effect", taking into account ICP, ECP, and reverse solute diffusion and comparing with experimental results.	PRO	Flat Sheet
[34]	They propose a total mass transfer coefficient that is composed of the mass transfer coefficients within the support layer, outside the support layer, and outside the active layer.	PRO	Flat sheet
[35]	Analytical solution to the differential equations governing the electrically coupled transport of three different ions through membrane barrier layers.	PRO	Flat Sheet
[36]	They drew a parallel between heat exchangers and PRO processes, considering the latter as mass exchangers. They define the recovery ratio, RR; the mass flux ratio, MR; the osmotic pressure ratio, SR; and the mass transfer unit number, MTU.	PRO	Flat sheet
[37,38]	A mathematical model for mass transport in PRO that considers mass transfer processes in the environments near the membrane, as well as in the active layer and support layer. The author begins by formulating solute flux for the four defined environments.	PRO	Flat Sheet
[39]	The solution–diffusion/pore flow/fluid resistance model. According to this model, the total resistance of the system to the transfer of solvent A is the sum of two resistances connected in series: the resistance of the membrane material (Am) and the resistance of the solution (As).	PRO	Flat Sheet
[40]	Considers the effect of ICP and ECP on both sides and the effect of reverse salt flux. The model was validated using lab-scale experiments and extended large-scale PRO membranes.	PRO	Flat Sheet.
[41]	Presents a mathematical model of solution–diffusion–convection (SDC), in which they consider the solute flux independently in the five interfaces that make up the system, which are the layers of the external environment, the active layer, the support layer, and a cake layer.	PRO	Flat Sheet
[42]	Evaluates the configurations AL-DS and AL-FS considering the costs of pretreatment and conclude that AL-FS could be better for Feed solutions prone to fouling like wastewater	PRO	Flat Sheet

Table A1. *Cont.*

Reference	Objective	Osmotic Process	Type of Membrane
[43]	Presents equations for the volumetric flow considering the membrane orientation, DECP, and CECP and evaluates the model against experimental data.	PRO	Flat Sheet
[44]	Presents a mathematical model of a scale-up PRO process capable of considering the increase in process scale and the detrimental effects, like CICP, DECP, and RSF.	PRO	Flat Sheet
[45]	Presents an analog electric circuit model representing PRO. The model considers RSF, CICP, and salt storage capacity of water.	PRO	Flat Sheet
[46]	Presents equations for a simplified square channel counter flow configuration. Present an equation for the diffusional resistance with pure water as feed solution and $\Delta P = 0$.	PRO	Tubular Membrane
[47]	Presents a model for an integrated seawater reverse osmosis (SWRO) and pressure-retarded osmosis (PRO). It considers components such as the SWRO unit, energy recovery device (ERD), PRO unit, high-pressure and low-pressure pumps, turbine, and others.	SWRO- PRO	Flat Sheet
[48]	Model for forward osmosis (FO) and pressure-retarded osmosis (PRO) based on irreversible thermodynamics (IT), specifically the Spiegler–Kedem (SK) model. This model includes three phenomenological parameters: the hydraulic permeability A, the solute permeability B, and a reflection coefficient σ that represents the convective effects or coupling effects in mass transport in the active layer of the membrane.	FO, PRO	Flat Sheet
[49]	Presents equations for flat sheet, hollow fiber, and double-skinned hollow fiber membranes, considering membrane orientation, DECP, and CICP.	PRO	Flat Sheet, Hollow Fiber, Dou- ble Skinned Hollow Fiber
[50]	Presents one-dimensional (1D) analytical equations for a parallel flow configuration in pressure-retarded osmosis (PRO) exchangers by using actual brine and feed salinity values from the Kuwait desalination industry. Uses mass transfer units.	PRO	Flat Sheet
[51]	Proposes a model to represent the difference between experimental and theoretical water flow and explain this difference with cavitation.	PRO	Flat Sheet
[52]	Proposes a model that considers cavitation and independence between the effects of feed and draw hydraulic pressures.	PRO	Flat Sheet
[53]	Depicts the limitations of a stand-alone PRO process and the effectiveness of a RO-PRO hybridized process.	PRO- RO	Flat Sheet, Hollow Fiber
[54]	Presents a model that describes an osmotic power station. It considers the relevant water and salt flows in the system. It also accounts for irreversible losses in the flow across the membrane as well as through the membrane unit, and in the surrounding pump–turbine system.	PRO	Flat Sheet

Table A1. *Cont.*

Reference	Objective	Osmotic Process	Type of Membrane
[55]	Presents models for scaled-up dual-stage PRO power plants compared to a single-stage PRO system with the same membrane area. These models consider the pressure and flow drop as well as the salinity change along the membrane. A thermodynamic analysis addresses the sources for irreversible losses and the contribution from each source.	PRO	Flat Sheet
[56,57]	Presents a simulator for PRO. The authors conduct various tests exploring the economic feasibility in terms of energy recovery for a PRO system. The simulator uses an electrolyte equation of state to obtain a more accurate calculation of osmotic pressures.	PRO	Flat Sheet
[58]	Studies the effects of mechanical stresses on the transport properties of thin-film composite (TFC) membranes used in osmotic processes. They propose a deformation coefficient that, when integrated into the solution–diffusion model, allows for representing the dependence of solute flux on the applied pressure, as has been observed experimentally.	PRO	Flat Sheet
[59]	Studies PRO using organic draw solutions at different temperatures and compares them with the results of NaCl as a draw solution. Their results indicate that organic salts allow one to obtain increased energy at higher temperatures coupled with lower reverse salt flux when compared to NaCl.	PRO	Flat Sheet
[60]	Simulates hybrid FO-RO and RO-PRO systems. Studies cross-flow and channel dimensions in spiral-wound modules. Defines a multi-stage recharge configuration for hybrid systems.	FO-RO, RO- PRO	Flat Sheet
[61]	Implemented an engineering-scale system for seawater desalination by reverse osmosis (RO) coupled with a PRO system (SWRO-PRO) to analyze the feasibility of PRO as an energy recovery element in RO. In this work, the authors propose a model they call solution–diffusion with defects (SDWD), in which the equations include a term to represent the volumetric fluxes and solute fluxes due to existing defects in the membranes.	SWRO- PRO	Flat Sheet
[62]	Compares the linear van ’t Hoff approach to the solutions using an OLI stream analyzer, which gives the real osmotic pressure values for various dilutions of NaCl solutions for FO and PRO. Compares the results from their model with experimental results.	FO, PRO	Flat Sheet
[63]	Investigates the significance of the energy generated by dual-stage pressure-retarded osmosis (DSPRO) from a reverse osmosis (RO) brine stream. The results demonstrate the potential of integrating the two pass RO with the DSPRO to reduce desalination’s energy consumption and environmental impacts.	2RO- DSPRO	Flat Sheet
[64]	Presents a module-scale model for spiral-wound membranes considering the dilution of high-salinity draw solutions along the spiral-wound module. The model explores the effects of the spiral-wound module glue line over the power density.	PRO	Flat Sheet

Table A1. *Cont.*

Reference	Objective	Osmotic Process	Type of Membrane
[65]	Investigates the concept of using heat to thermally enhance pressure-retarded osmosis for improved energy recovery from salt gradients. It is found that although operation at higher temperatures may yield higher power, operation at low temperatures of 30∘C may represent a more effective use of thermal energy.	PRO	Flat Sheet
[2]	Investigates the effects of intrinsic membrane parameters on DECP during FO.In particular, the Peclet number is utilized to evaluate the degree of DECP.	FO,	Flat Sheet
[66]	Explores the concept of high pressure with hypersaline solutions for a hybrid SWRO system. This work states that it is possible to achieve high power densities with a mix of seawater as a feed solution and hypersaline water as a draw solution. This increments the requirements for the structural parameters of the membrane and increments the negative effects of CICP.	SWRO-	Flat Sheet
[67]	Presents a 1-dimensional model of a spiral-wound membrane module in a counter-current flow configuration and assesses the impact of feed solution pretreatment on the energy output.	PRO	Flat Sheet

References

1. Tawalbeh, M.; Al-Othman, A.; Abdelwahab, N.; Alami, A.H.; Olabi, A.G. Recent developments in pressure retarded osmosis for desalination and power generation. *Renew. Sustain. Energy Rev.* **2021**, *138*, 110492. [CrossRef]
2. Chae, S.H.; Rho, H.; Moon, S. Modeling study of the effects of intrinsic membrane parameters on dilutive external concentration polarization occurring during forward and pressure-retarded osmosis. *Desalination* **2024**, *569*, 117043. [CrossRef]
3. Ruiz-García, A.; Tadeo, F.; Nuez, I. Role of permeability coefficients in salinity gradient energy generation by PRO systems with spiral wound membrane modules. *Renew. Energy* **2023**, *215*, 118954. [CrossRef]
4. Zhang, J.X.; Tian, T.; Du, W.J.; Guan, Y.F.; Wang, Y.J.; Li, Y.S.; Yu, H.Q. Adopting vibration to alleviate the solute buildup and membrane fouling in a forward osmosis system. *J. Clean. Prod.* **2021**, *323*, 129202. [CrossRef]
5. Binger, Z.M.; Achilli, A. Surrogate modeling of pressure loss & mass transfer in membrane channels via coupling of computational fluid dynamics and machine learning. *Desalination* **2023**, *548*, 116241. [CrossRef]
6. Chai, M.; Ye, Y.; Razmjou, A.; Chen, V. Insights into the mass transfer improvement of a submerged forward osmosis system with vibration-induced shear enhancement. *Ind. Eng. Chem. Res.* **2021**, *60*, 1375–1386. [CrossRef]
7. Kastl, A.; Bar-Zeev, E.; Spinnler, M.; Sattelmayer, T. Impact of pulsating flows on particle deposition in forward osmosis with spacers. *J. Membr. Sci.* **2021**, *635*, 119444. [CrossRef]
8. Wang, J.M.; Jin, Q.Q.; Zhang, Y.Y.; Fang, H.C.; Xia, H.M. Reducing the membrane fouling in cross-flow filtration using a facile fluidic oscillator. *Sep. Purif. Technol.* **2021**, *272*, 118854. [CrossRef]
9. Wild, P.M.; Vickers, G.W.; Djilali, N. The fundamental principles and design considerations for the implementation of centrifugal reverse osmosis. *Proc. Inst. Mech. Eng. Part E J. Process Mech. Eng.* **1997**, *211*, 67–81. [CrossRef]
10. Pharoah, J.G.; Djilali, N.; Vickers, G.W. Fluid mechanics and mass transport in centrifugal membrane separation. *J. Membr. Sci.* **2000**, *176*, 277–289. [CrossRef]
11. Bergen, A.; Fyles, T.M.; Lycon, D.S.; Vickers, G.W.; Wild, P. Flux enhancement in reverse osmosis using centrifugal membrane separation. *J. Membr. Sci.* **2000**, *176*, 257–266. [CrossRef]
12. Lee, S.; Lueptow, R.M. Rotating reverse osmosis: A dynamic model for flux and rejection. *J. Membr. Sci.* **2001**, *192*, 129–143. [CrossRef] [PubMed]
13. Lee, S.; Lueptow, R.M. Control of scale formation in reverse osmosis by membrane rotation. *Desalination* **2003**, *155*, 131–139. [CrossRef]
14. Krantz, W.B.; Chong, T.H. Centrifugal reverse osmosis (CRO) a novel energy-efficient membrane process for desalination near local thermodynamic equilibrium. *J. Membr. Sci.* **2021**, *637*, 119630. [CrossRef]

15. Wijmans, J.G.; Baker, R.W. *The Solution-Diffusion Model: A Unified Approach to Membrane Permeation*; John Wiley & Sons, Ltd.: Hoboken, NJ, USA, 2006; pp. 159–189. [CrossRef]
16. Nagy, E. *Basic Equations of Mass Transport Through a Membrane Layer*; Elsevier Inc.: Amsterdam, The Netherlands, 2018; pp. 1–545. [CrossRef]
17. Lee, K.L.; Baker, R.W.; Lonsdale, H.K. Membranes for power generation by pressure-retarded osmosis. *J. Membr. Sci.* **1981**, *8*, 141–171. [CrossRef]
18. Sharqawy, M.H.; Lienhard, V.J.H.; Zubair, S.M. Thermophysical properties of seawater: A review of existing correlations and data. *Desalination Water Treat.* **2010**, *16*, 354–380. [CrossRef]
19. Abdelkader, B.A.; Navas, D.R.; Sharqawy, M.H. A novel spiral wound module design for harvesting salinity gradient energy using pressure retarded osmosis. *Renew. Energy* **2023**, *203*, 542–553. [CrossRef]
20. Attarde, D.; Jain, M.; Chaudhary, K.; Gupta, S.K. Osmotically driven membrane processes by using a spiral wound module—Modeling, experimentation and numerical parameter estimation. *Desalination* **2015**, *361*, 81–94. [CrossRef]
21. Wijmans, J.G.; Baker, R.W. The solution-diffusion model: A review. *J. Membr. Sci.* **1995**, *107*, 1–21. [CrossRef]
22. Loeb, S.; Van Hessen, F.; Shahaf, D. Production of energy from concentrated brines by pressure-retarded osmosis. II. Experimental results and projected energy costs. *J. Membr. Sci.* **1976**, *1*, 249–269. [CrossRef]
23. Mehta, G.D.; Loeb, S. Internal polarization in the porous substructure of a semipermeable membrane under pressure-retarded osmosis. *J. Membr. Sci.* **1978**, *4*, 261–265. [CrossRef]
24. Loeb, S.; Mehta, G.D. A two-coefficient water transport equation for pressure-retarded osmosis. *J. Membr. Sci.* **1978**, *4*, 351–362. [CrossRef]
25. McCutcheon, J.R.; Elimelech, M. Influence of concentrative and dilutive internal concentration polarization on flux behavior in forward osmosis. *J. Membr. Sci.* **2006**, *284*, 237–247. [CrossRef]
26. McCutcheon, J.R.; Elimelech, M. Modeling water flux in forward osmosis: Implications for improved membrane design. *AIChE J.* **2007**, *53*, 1736–1744. [CrossRef]
27. Achilli, A.; Cath, T.Y.; Childress, A.E. Power generation with pressure retarded osmosis: An experimental and theoretical investigation. *J. Membr. Sci.* **2009**, *343*, 42–52. [CrossRef]
28. Thorsen, T.; Holt, T. The potential for power production from salinity gradients by pressure retarded osmosis. *J. Membr. Sci.* **2009**, *335*, 103–110. [CrossRef]
29. Xu, Y.; Peng, X.; Tang, C.Y.; Fu, Q.S.; Nie, S. Effect of draw solution concentration and operating conditions on forward osmosis and pressure retarded osmosis performance in a spiral wound module. *J. Membr. Sci.* **2010**, *348*, 298–309. [CrossRef]
30. Yip, N.Y.; Elimelech, M. Performance limiting effects in power generation from salinity gradients by pressure retarded osmosis. *Environ. Sci. Technol.* **2011**, *45*, 10273–10282. [CrossRef]
31. Sivertsen, E.; Holt, T.; Thelin, W.; Brekke, G. Modelling mass transport in hollow fibre membranes used for pressure retarded osmosis. *J. Membr. Sci.* **2012**, *417–418*, 69–79. [CrossRef]
32. She, Q.; Jin, X.; Li, Q.; Tang, C.Y. Relating reverse and forward solute diffusion to membrane fouling in osmotically driven membrane processes. *Water Res.* **2012**, *46*, 2478–2486. [CrossRef] [PubMed]
33. Kim, Y.C.; Elimelech, M. Adverse impact of feed channel spacers on the performance of pressure retarded osmosis. *Environ. Sci. Technol.* **2012**, *46*, 4673–4681. [CrossRef] [PubMed]
34. She, Q.; Wong, Y.K.W.; Zhao, S.; Tang, C.Y. Organic fouling in pressure retarded osmosis: Experiments, mechanisms and implications. *J. Membr. Sci.* **2013**, *428*, 181–189. [CrossRef]
35. Yaroshchuk, A.; Bruening, M.L.; Licón Bernal, E.E. Solution-Diffusion-Electro-Migration model and its uses for analysis of nanofiltration, pressure-retarded osmosis and forward osmosis in multi-ionic solutions. *J. Membr. Sci.* **2013**, *447*, 463–476. [CrossRef]
36. Sharqawy, M.H.; Banchik, L.D.; Lienhard, J.H. Effectiveness-mass transfer units (ϵ-MTU) model of an ideal pressure retarded osmosis membrane mass exchanger. *J. Membr. Sci.* **2013**, *445*, 211–219. [CrossRef]
37. Nagy, E. A general, resistance-in-series, salt- and water flux models for forward osmosis and pressure-retarded osmosis for energy generation. *J. Membr. Sci.* **2014**, *460*, 71–81. [CrossRef]
38. Nagy, E.; Hajba, L.; Prettl, Z. Modelling and prediction of renewable energy generation by pressure retarded osmosis. *Comput. Aided Chem. Eng.* **2014**, *33*, 1105–1110. [CrossRef]
39. Sharif, A.O.; Merdaw, A.A.; Aryafar, M.; Nicoll, P. Theoretical and experimental investigations of the potential of osmotic energy for power production. *Membranes* **2014**, *4*, 447–468. [CrossRef]
40. Touati, K. Energy Generation and Recovery by Pressure Retarded Osmosis (PRO): Modeling and Experiments. Ph.D. Thesis, Universidad de Valladolid, Valladolid, Spain, 2015.

41. Nagy, E.; Dudás, J.; Hegedüs, I. Improvement of the energy generation by pressure retarded osmosis. *Energy* **2016**, *116*, 1323–1333. [CrossRef]
42. Kim, J.; Park, M.J.; Park, M.; Shon, H.K.; Kim, S.H.; Kim, J.H. Influence of colloidal fouling on pressure retarded osmosis. *Desalination* **2016**, *389*, 207–214. [CrossRef]
43. Nguyen, T.P.N.; Jun, B.M.; Park, H.G.; Han, S.W.; Kim, Y.K.; Lee, H.K.; Kwon, Y.N. Concentration polarization effect and preferable membrane configuration at pressure-retarded osmosis operation. *Desalination* **2016**, *389*, 58–67. [CrossRef]
44. He, W. Modelling, Optimisation and Control of Osmotic Energy Extraction from Natural Salinity Gradients Using Pressure Retarded Osmosis. Ph.D. Thesis, Queen Mary, University of London, London, UK, 2016.
45. Maisonneuve, J.; Pillay, P.; Maisonneuve, J.; Pillay, P. Analog electric circuit representation of energy conversion by pressure retarded osmosis. In Proceedings of the 2016 IEEE Power and Energy Society General Meeting (PESGM), Boston, MA, USA, 17–21 July 2016. [CrossRef]
46. Anissimov, Y.G. Aspects of mathematical modelling of pressure retarded osmosis. *Membranes* **2016**, *6*, 13. [CrossRef] [PubMed]
47. Senthil, S.; Senthilmurugan, S. Reverse Osmosis-Pressure Retarded Osmosis hybrid system: Modelling, simulation and optimization. *Desalination* **2016**, *389*, 78–97. [CrossRef]
48. Attarde, D.; Jain, M.; Gupta, S.K. Modeling of a forward osmosis and a pressure-retarded osmosis spiral wound module using the Spiegler-Kedem model and experimental validation. *Sep. Purif. Technol.* **2016**, *164*, 182–197. [CrossRef]
49. Cheng, Z.L.; Chung, T.S. Mass transport of various membrane configurations in pressure retarded osmosis (PRO). *J. Membr. Sci.* **2017**, *537*, 160–176. [CrossRef]
50. Al-Anzi, B.S.; Thomas, A. One-dimensional analytical modeling of pressure-retarded osmosis in a parallel flow configuration for the desalination industry in the State of Kuwait. *Sustainability* **2018**, *10*, 1288. [CrossRef]
51. Gao, N.; Wang, J.; Song, L. Independence of hydraulic pressures on the feed and draw solutions in the osmotically driven membrane processes. *J. Membr. Sci.* **2019**, *586*, 1–6. [CrossRef]
52. Zhang, N.; Yin, S.Y.; Yang, H.H. Transient performance of coupled heat and mass transfer in cross-flow hollow fiber membrane module for air dehumidification. *Int. J. Refrig.* **2019**, *108*, 190–199. [CrossRef]
53. Ho Chae, S.; Kim, Y.M.; Park, H.; Seo, J.; Lim, S.J.; Kim, J.H. Modeling and simulation studies analyzing the pressure-retarded osmosis (PRO) and pro-hybridized processes. *Energies* **2019**, *12*, 243. [CrossRef]
54. Di Michele, F.; Felaco, E.; Gasser, I.; Serbinovskiy, A.; Struchtrup, H. Modeling, simulation and optimization of a pressure retarded osmosis power station. *Appl. Math. Comput.* **2019**, *353*, 189–207. [CrossRef]
55. Soltani, R.; Struchtrup, H. Modeling and simulation of the dual stage pressure retarded osmosis systems. *Desalination* **2019**, *460*, 28–40. [CrossRef]
56. Manzoor, H.; Selam, M.A.; Adham, S.; Shon, H.K.; Castier, M.; Abdel-Wahab, A. Energy recovery modeling of pressure-retarded osmosis systems with membrane modules compatible with high salinity draw streams. *Desalination* **2020**, *493*, 114624. [CrossRef]
57. Manzoor, H.; Selam, M.A.; Abdur Rahman, F.B.; Adham, S.; Castier, M.; Abdel-Wahab, A. A tool for assessing the scalability of pressure-retarded osmosis (PRO) membranes. *Renew. Energy* **2020**, *149*, 987–999. [CrossRef]
58. Idarraga-Mora, J.A.; O'Neal, A.D.; Pfeiler, M.E.; Ladner, D.A.; Husson, S.M. Effect of mechanical strain on the transport properties of thin-film composite membranes used in osmotic processes. *J. Membr. Sci.* **2020**, *615*, 118488. [CrossRef]
59. Adhikary, S.; Islam, M.S.; Touati, K.; Sultana, S.; Ramamurthy, A.S.; Rahaman, M.S. Increased power density with low salt flux using organic draw solutions for pressure-retarded osmosis at elevated temperatures. *Desalination* **2020**, *484*, 114420. [CrossRef]
60. Binger, Z.M.; Achilli, A. Forward osmosis and pressure retarded osmosis process modeling for integration with seawater reverse osmosis desalination. *Desalination* **2020**, *491*, 114583. [CrossRef]
61. Binger, Z.M.; O'Toole, G.; Achilli, A. Evidence of solution-diffusion-with-defects in an engineering-scale pressure retarded osmosis system. *J. Membr. Sci.* **2021**, *625*, 119135. [CrossRef]
62. Nagy, E.; Hegedüs, I.; Rehman, D.; Wei, Q.J.; Ahdab, Y.D.; Lienhard, J.H. The need for accurate osmotic pressure and mass transfer resistances in modeling osmotically driven membrane processes. *Membranes* **2021**, *11*, 128. [CrossRef]
63. Al-Zainati, N.; Subbiah, S.; Yadav, S.; Altaee, A.; Bartocci, P.; Ibrar, I.; Zhou, J.; Samal, A.K.; Fantozzi, F. Experimental and theoretical work on reverse osmosis—Dual stage pressure retarded osmosis hybrid system. *Desalination* **2022**, *543*, 116099. [CrossRef]
64. Matta, S.M.; Selam, M.A.; Manzoor, H.; Adham, S.; Shon, H.K.; Castier, M.; Abdel-Wahab, A. Predicting the performance of spiral-wound membranes in pressure-retarded osmosis processes. *Renew. Energy* **2022**, *189*, 66–77. [CrossRef]
65. Chintalacheruvu, S.; Ren, Y.; Maisonneuve, J. Effectively using heat to thermally enhance pressure retarded osmosis. *Desalination* **2023**, *556*, 116570. [CrossRef]

66. Lee, J.; Shin, Y.; Kim, J.; Hong, S. Feasibility and challenges of high-pressure pressure retarded osmosis applications utilizing seawater and hypersaline water sources. *Desalination* **2024**, *581*, 117578. [CrossRef]
67. Tagliavini, M.; Babler, M.U. Simulation of spiral-wound pressure retarded osmosis for harvesting osmotic power: Module-level modeling and implications of feed pre-treatment. *Desalination* **2024**, *574*, 117184. [CrossRef]

Disclaimer/Publisher's Note: The statements, opinions and data contained in all publications are solely those of the individual author(s) and contributor(s) and not of MDPI and/or the editor(s). MDPI and/or the editor(s) disclaim responsibility for any injury to people or property resulting from any ideas, methods, instructions or products referred to in the content.